Heliyon

Received:
9 January 2018
Revised:
5 March 2018
Accepted:
23 March 2018

Cite as: Mandee Yang, Grace Eun Nam, Atriya Salamati, Michael Baldwin, Mengzhao Deng, Zi-Jun Liu. Alveolar bone loss and mineralization in the pig with experimental periodontal disease.
Heliyon 4 (2018) e00589.
doi: 10.1016/j.heliyon.2018.e00589

Alveolar bone loss and mineralization in the pig with experimental periodontal disease

Mandee Yang [a,1], **Grace Eun Nam** [a,1], **Atriya Salamati** [a,b], **Michael Baldwin** [a,b], **Mengzhao Deng** [a,c], **Zi-Jun Liu** [a,b,*]

[a] *Dept. Orthodontics, School of Dentistry, University of Washington, Seattle, USA*

[b] *Dept. Oral Health Sciences, School of Dentistry, University of Washington, Seattle, USA*

[c] *State Key Laboratory of Oral Diseases, West China Hospital of Stomatology, Sichuan University, Chengdu 610041, PR China*

[*] Corresponding author.
E-mail address: zjliu@uw.edu (Z.-J. Liu).

[1] Equally contributed.

Abstract

Objective: To address how experimental periodontal disease affects alveolar bone mass and mineral apposition in a young pig model.

Materials and methods: Seven three-month-old pigs were periodically inoculated with 4 types of periodontal bacteria, along with a ligature around the last maxillary deciduous molar for 8 weeks to induce periodontal disease (PG). Eight same-aged pigs served as the control (CG). Segmentations of 3D cone-beam CT images were performed to quantify volumes of the total alveolar bone, alveolar ridge, and all roots of the target molar. Calcein and alizarin were administered for labeling mineral apposition before euthanasia. The harvested molar blocks were sectioned and examined under epifluorescence. The inter-label distance between the two vital markers at regional bone surfaces were measured and mineral apposition rate (MAR) was calculated.

Results: A significant reduction of total alveolar bone volume was seen in PG with the major loss at the alveolar ridge. MAR was significantly higher at the root furcation region than those at both buccal and palatal ridges in CG. Compared

https://doi.org/10.1016/j.heliyon.2018.e00589

with CG, PG animals showed more interrupted labeled bands with significantly lower MAR at the furcation region. MARs were positively associated with both the volumes of total alveolar bone and ridge in CG, but only with the total alveolar bone in PG.

Conclusions: In young growing pigs, mineral apposition is region specific. The experimental periodontal disease not only leads to alveolar bone loss, but also perturbs mineral apposition for new bone formation, thus impairing the homeostasis of alveolar bone remodeling.

Keyword: Dentistry

1. Introduction

Periodontal disease is a serious infection that damages soft and hard tissues of the periodontium, including the alveolar bone, thus the destruction of alveolar bone is a hallmark of periodontal disease. A number of studies have placed a focus on how inflammation from the periodontal disease and involving bacteria leads to alveolar bone loss through various proinflammatory molecules and cytokine networks (Di Benedetto et al., 2013; Henderson and Kaiser, 2018; Hienz et al., 2015), and other studies characterized additional features of alveolar bone loss resulting from periodontal disease (Cochran, 2008). Since coupled bone resorption and formation is the key mechanism to maintain homeostasis of the healthy skeletal system (Hienz et al., 2015; Rodan, 1998), excessive alveolar bone resorption may be compensated by more active bone formation to restore or preserve the homeostatic status. However, this homeostatic mechanism could be perturbed by the existence of destructive proinflammatory molecules and cytokines along with mechanic traumas from altered occlusion in periodontal disease, tipping the balance in favor of bone resorption over bone formation (Hienz et al., 2015; Rodan and Martin, 2000). Due to this imbalance, bone loss takes place and the reduction of regional mineralization is anticipated. Although matrix vesicle and nuleation theories have been proposed for calcification process in the formation of new bone (Hienz et al., 2015), few studies have addressed how alveolar bone loss is related to the bone calcification process through regional mineralization in periodontal disease. This knowledge gap prevents us from better understanding the mechanism of bone pathophysiology in periodontal disease. Therefore, the purpose of the current study was to quantify the regional bone loss *vs* regional mineral apposition on alveolar bone in a young pig model with experimental periodontal disease. It is hypothesized that mineral apposition at the surfaces of alveolar bone is region-specific in normal growth and remodeling, but experimental periodontal disease impedes this process, distorting the normal interactions between alveolar bone loss and mineral apposition.

https://doi.org/10.1016/j.heliyon.2018.e00589

2. Methods

2.1. Animals and the induction of periodontal disease

Due to the great similarity of a pig's dental and periodontal anatomy to that of humans, including both the comparable size and jaw/teeth function (Herring et al., 2011), 15 juvenile (3-month-old) farm pigs were obtained from Progressive Swine Farms (Woodinville, WA). Seven of those pigs were subjected to the induction of experimental periodontal disease (periodontal group, PG) bilaterally (n = 3) or unilaterally (n = 4, split mouth experiment, the induction side was determined by the coin toss). The rest of the 8 pigs served as the control group (CG).

Under intubated anesthesia with isoflurane, a ligature (3-0 silk braided suture) was placed around the last maxillary molar with buccal and palatal overhang composite markers. These markers served as landmarks for initial gingival height, allowing longitudinal measures of the changes in alveolar ridge height, and also facilitated dental plaque accumulation and ligature retention. After ligature placement, 4 types of periodontal bacteria (*P. gingivalis, S. gordonii, A. actinomycetemcomitans, and F. nucleatum*) were inoculated around the ligature. The rationale for selecting these 4 types of bacteria were based on literature reports (Farquharson et al., 2012; Henderson and Kaiser, 2018; Meng et al., 1996; Oz and Puleo, 2011). The ligature was mornitored and bacteria cocktail was refreshed twice a week. Dental apical radiography (PA), perio-charting and probing were performed weekly for a period of 8 weeks. Six-site perio-charting was performed same as in clinic, and dental plaque and bleeding upon probing were scored. Regular pig chow was offered throughout the experimental period, and the body weights were tracked weekly. The animal protocol was approved by the Institutional Animal Care and Use Committee, University of Washington (Protocol# 3393-03).

2.2. Cone-beam CT images and bone labeling markers

Upon arrival, all pigs received cone-beam CT imaging (CBCT, Morita Accuitomo 170, Kyoto, Japan). An intubated pig was secured on a modified car seat, which was placed on the CBCT chair (Fig. 1). The settings for the CBCT were 90 kV, 5.0 mA, and a voxel resolution of 270 μm, with the central beam localized at the upper molar area. The CBCT images were performed again on all PG pigs immediately after the terminal experiment. In addition, the molar segments that were harvested after euthanasia were μCT scanned (Skyscan 1076, Bruker, Kontich, Belgium) for measurements of 3D periodontal spaces (the results will be reported elsewhere).

Pigs were injected with calcein (20 mg/kg) and alizarin complexone (30 mg/kg) (Sigma Chemical, St. Louis, MO, USA) intravenously 7 and 2 days respectively, prior to the terminal experiment (Liu et al., 2006). These fluorescent dyes chelate to calcium ions, resulting in deposition of a double vital label on all actively

https://doi.org/10.1016/j.heliyon.2018.e00589

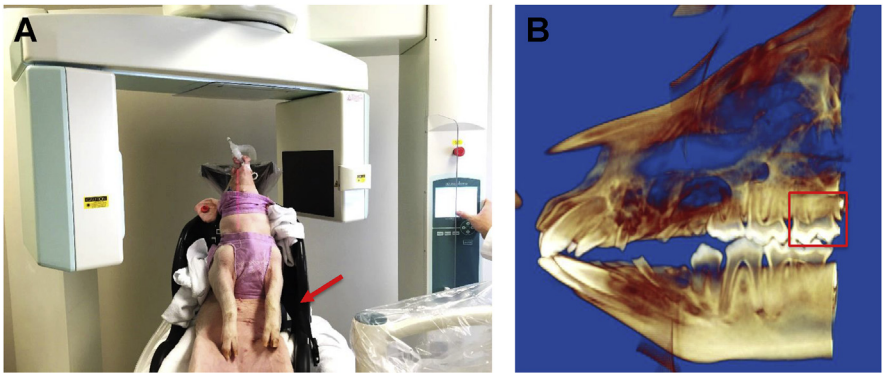

Fig. 1. A: A live pig receives the CBCT imaging. The arrow indicates the custom-made chair for stabilizing the position of the pig. B: Reconstructed 3D CBCT image. The red box indicates the target molar.

mineralizing bone surfaces. After euthanasia, upper molar blocks of both sides were removed from the cadavers and fixed in 10% formalin. The left undecalcified molar blocks were embedded in micro-bed embedding resin following the protocol provided by the manufacturer (EMS Co., Fort Washington, PA, USA), while the right molar blocks were decalcified for the histological and immunohistochemical investigations (the results will be reported elsewhere). Successive coronal sections from the distal region of the molar blocks were taken at thicknesses of 30 μm using a Leica SP1600 saw microtome (Leica Microsystem, Bannockburn, IL, USA) and mounted on 1% gelatinized slides. These sections were examined unstained under epifluorescence with the aid of a Nikon Eclipse E400 microscope (Nikon Corporation, Tokyo, Japan) with a Spot RT digital camera. Images were captured at 4X magnification with the use of Metavue software (Universal Imaging Corporation, Downingtown, PA, USA). Green (calcein) and red (alizarin complexone) images were captured separately and then merged. After adjusting for brightness/contrast and size calibration, a series of merged images with the double-labeled bone surfaces were saved for measurements (Fig. 2).

2.3. CBCT image and bone labelling measurements

CBCT images were used to create 3D models using the software ITK-Snap (www.itksnap.org) with the aid of Invivo5 (Anatomage Co., San Jose, CA) for the orientation adjustment. The semi-automatic algorithm of the software was guided by visually identifying the maxillary molar region from the displayed DICOM image. The software aided the visual selection by orienting the DICOM image to the region of interest (ROI) in all sliced images. The segmentation process started by selecting the ROI in all x, y and z directions and the software assigning an integer value to each voxel size in the image volume. Manual segmentation, consisting of the "polygon" and "paint brush tools", was done to delete any imperfections created by the software that were created by the image noise in the DICOM images

https://doi.org/10.1016/j.heliyon.2018.e00589

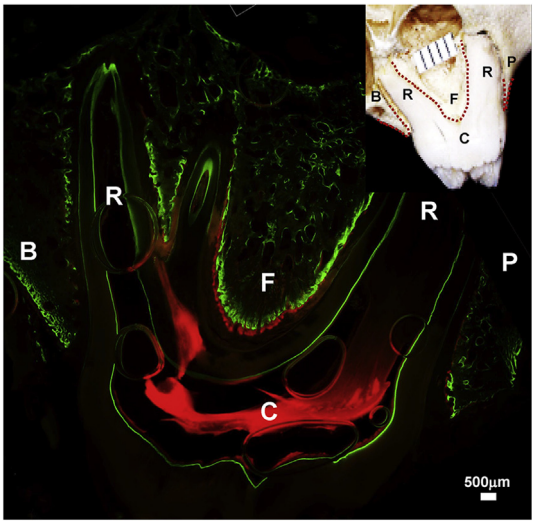

Fig. 2. A bone-labeled section under epifluorescence. The dotted red lines in the insert of the right-upper corner indicate the surfaces measured for mineral apposition rate (MAR). B: buccal alveolar ridge; P: palatal alveolar ridge; F: region underneath the root furcation; C: molar crown; R: molar root.

(Yushkevich et al., 2006). The segmentations were performed using the following anatomic landmarks: 1) crown and root were separated at the cemento-enamel junction (CEJ) of the target molar; 2) total alveolar bone surrounding the target molar was defined from the CEJ to 2 mm below each root apex of the target molar; 3) the alveolar ridge was defined 2.5 mm apically from the CEJ, then further divided into buccal and palatal ridges by the central line of the target molar sagittally. Thus, the volumetric calculations were for the following variables: total roots, total alveolar bone, total alveolar ridge, and buccal and palatal alveolar ridges (Fig. 3). The observer (GN) was blinded to the group and time point assignments. The volumetric calculations of both sides were performed for control and bilateral induction animals, and induction and control sides for unilateral induction animals. For all PG animals, the volumetric calculations were performed for both CBCT images taken before and after the induction of periodontal disease.

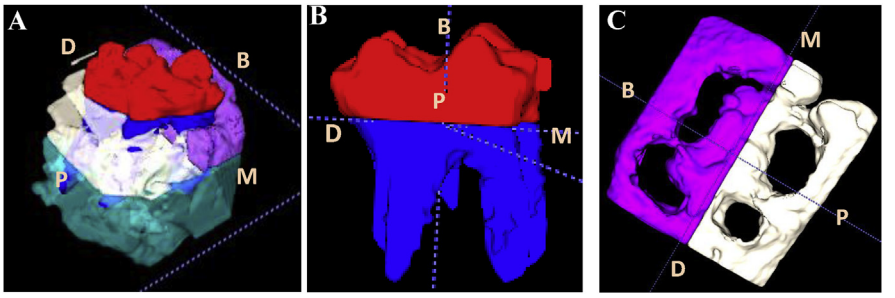

Fig. 3. Segmentations of 3D model of CBCT image. A: Color assignments for different portion of target molar and surrounding alveolar bone; B: Segmented molar from alveolar bone. Red and blue colors indicate molar crown and roots, respectively. C: Segmented alveolar ridge, purple and white colors indicate buccal and palatal ridges, respectively. M: mesial; D: distal; B: buccal; P: palatal.

https://doi.org/10.1016/j.heliyon.2018.e00589

For vital bone labeling measurements, a series of circles (50−120 for each alveolar ridge surface, and 15−30 for the surface underneath the root furcation), tangent to the lines delineating each color band of the labels, were superimposed over each merged image between the calcein (green) and the alizarin (red) bands, and these circles were lined up successively to cover the entire band defined by the two lines (Liu et al., 2006). The amount of bone surface measured was defined by a distance of 1,000 pixels (2.44 mm) from the crest of the ridge and 500 pixels from the top of the furcation (1.22 mm) (Fig. 4). The diameter of each circle was logged directly into an Excel file with the use of Metavue Research Imaging Software (Molecular Devices LLC, San Jose, CA), and means were calculated. These values represented the inter-label distance, and were divided by the time interval between administrations of the two vital markers (2 days) to calculate mineral apposition rate (MAR). This nomenclature and calculation are in accordance with the American Society of Bone and Mineral Research Histomorphometry Nomenclature Committee (Dempster et al., 2013). To reduce the unavoidable variation in sectioning orientation resulting from embedding procedures, three successive sections that contained the most intact buccal and palatal roots of the target molar from each block were selected and examined under epifluorescence, and the measured values were averaged. The observer (MY) was blinded to the group assignment.

2.4. Data summary and statistics

The intra- and inter-examiner reliabilities of the volumetric calculations upon the segmentations on CBCT images were assessed by analyzing the difference between duplicate measurements taken at 10 days apart by the same observer (GN), and by two different observers (GN and MD) on 4 images. A paired t-test indicated that there was no significant difference ($p > 0.05$) between the measurements by the two observers, and the Dahlberg formula (Dahlberg, 1940) indicated that the intra-examiner error was less than 2%. Since the volumetric calculations from both sides in control and bilateral induction animals did not show the significant differences between sides, the values were averaged for each animals.

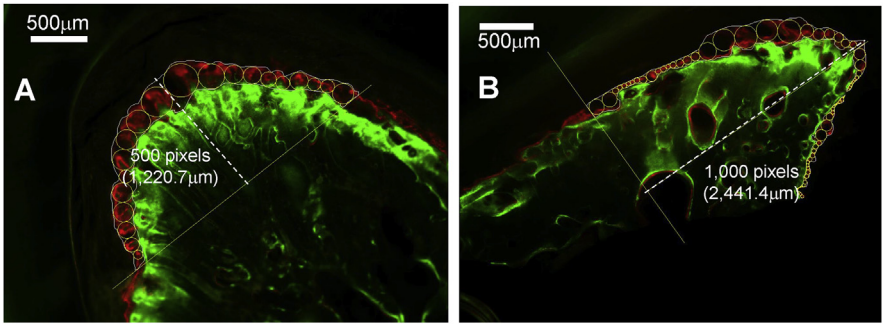

Fig. 4. Method of mineral apposition rate (MAR) measurements. A: The region underneath the root furcation; B: Alveolar ridge. The dotted lines define the heights of measured regions.

https://doi.org/10.1016/j.heliyon.2018.e00589

Giving the fact that bone mass and tooth size are closely related to body size (Anderson et al., 1977; Gingerich, 1977), the volumetric calculations for PG pigs after the induction were adjusted individually by their 8-week body weight gains in order to make the comparison before and after the induction of periodontal disease.

Descriptive data was first examined for distribution using a statistical package (ver. 19.0; SPSS Inc., Chicago, IL, USA), and parametric statistical approaches were applied for the CBCT data as these volumetric values were normally distributed. One-way ANOVA was used to detect overall differences between CG, PG before, and PG after the induction. The Tukey post-hoc tests were further used to detect pair-wise differences. Due to the large variations of MAR values, a non-parametric test (independent samples) was carried out to compare MAR values between CG and PG after the induction, as the samples from PG before the induction were not available. Non-parametric Spearman correlation analysis was applied to examine the associations between regional bone loss and mineral apposition. Significance level was set at $p < 0.05$ for both parametric and non-parametric tests.

3. Results

3.1. Assessments of induction of experimental periodontal disease

Five to six weeks after the induction, significant plaque accumulations were seen around the ligated molar with severe bleeding upon probing, and sometimes pus discharge appeared. Periodical charting clearly demonstrated the formation of deep periodontal pockets. Compared with the same molar of the control side in the unilateral induction animals, significantly deeper periodontal pocket of both buccal and palatal sides were charted starting from 10−12 days after the induction, and the pockets were deeper than 4 mm 17−22 days after the induction (Fig. 5A). The same periocharting and probing in the adjacent 2nd molar indicated that there was no visible plaque accumulation, bleeding from probing, or deeper periodontal pocket (Fig. 5B). The bilateral induction animals showed the periodontal pockets with similar depths. In both bilateral and unilateral induction animals over the period of 8 weeks, the alveolar ridge heights around the ligated molar were decreased significantly with a range of 2.7−5.9 mm in both PA dental films and CBCT images, but those around the adjacent 2nd molar were not affected with 0−1.5 mm height changes.

Although experimental periodontal disease was successfully induced over time, this disease seemed to have no effect on general health, because weekly body weight tracking for the PG indicated that the body weight continued to increase over time with a 29−59% weight gain by the end of 8 weeks (Fig. 6).

https://doi.org/10.1016/j.heliyon.2018.e00589

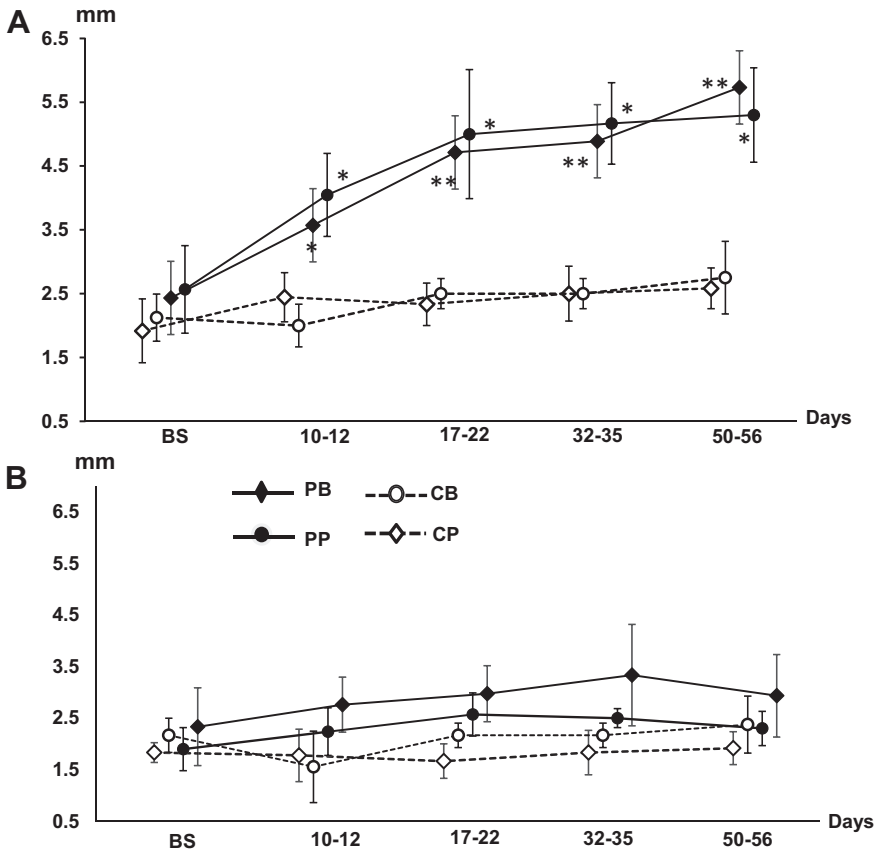

Fig. 5. The curves of periodontal pocket depths (Periocharting) over time in PG animals. A: The last deciduous upper molar (the target molar); B: The adjacent second deciduous upper molars. PB/PP: Buccal and palatal pocket depths of the induced side molars: CB/CP: buccal and palatal pockets depths of the control side molars. Error whiskers across each curve indicate standard deviations (SDs) at each time point. Asterisks indicate significant levels when the induced was compared with control sides. *$p < 0.05$; **$p < 0.01$.

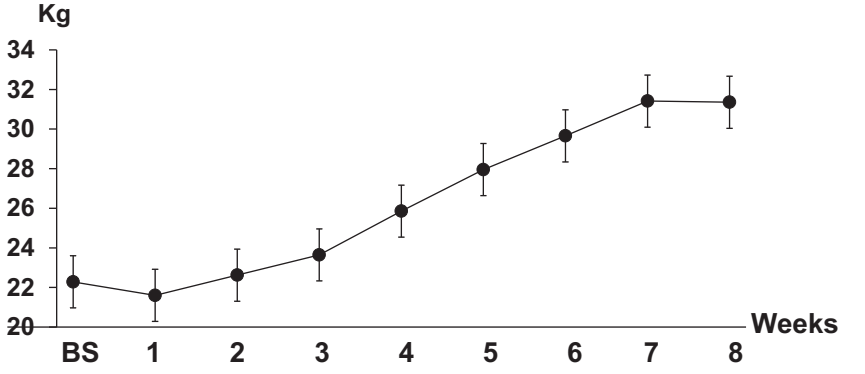

Fig. 6. The curve of body weight gain over time in PG animals. BS: base line. Error whiskers across the curve indicate standard deviations (SDs) at each time point.

https://doi.org/10.1016/j.heliyon.2018.e00589

3.2. Changes in alveolar bone mass and molar roots

There were no significant differences in all measured volumes of alveolar bone (total, all ridge, buccal and palatal ridges) between the CG and the PG before the induction (PGb, Fig. 7A and C). However, the PG after the induction (PGa) showed significant smaller total and palatal ridges as compared with the CG and the PGb, and overall buccal ridge volumes were larger than those of palatal ridges in all 3 groups (Fig. 7C). Interestingly, all-root volumes of the PGa were reduced significantly as compared to those of the CG and the PGb (Fig. 7B).

3.3. Changes in regional mineralization rates of alveoli

Mineralization bands were clearly seen in all regional surfaces of alveoli but the bands were disrupted more frequently in the sections of the PGa (Fig. 8). As shown in Fig. 9, the highest MAR was found in the region under the root furcation in both the CG and PGa animals, and the MAR of this region is significantly higher than all other measured regions except for the buccal surface of the buccal ridge (B-B) in the CG. There is a clear trend that the MAR of the PGa was smaller at each measured region than those of the CG, and significantly lower at the region underenath the root furcation (Fig. 9, left boxplots). The results also indicated that MARs were

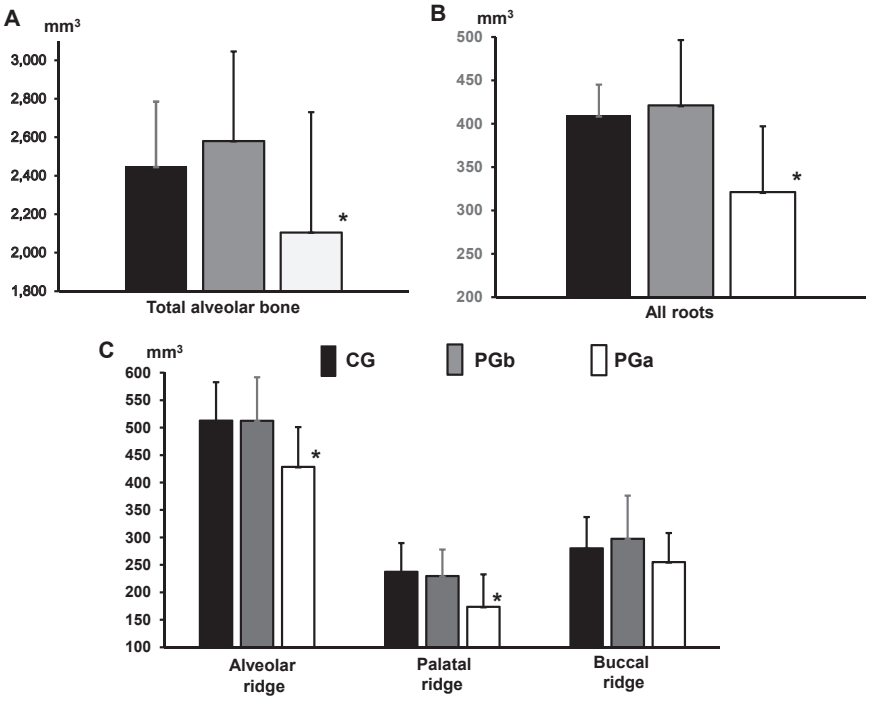

Fig. 7. Volumetric comparisons of total alveolar bone (A), all roots (B), and alveolar ridge (C). CG: control group; PGb and PGa: experimental group before and 8 weeks after the induction of periodontal disease, respectively. Error whiskers above each bar indicate standard deviations (SDs) in each group. Asterisk above the PGa histograms indicates $p < 0.05$ when PGa were compared with CG or PGb.

https://doi.org/10.1016/j.heliyon.2018.e00589

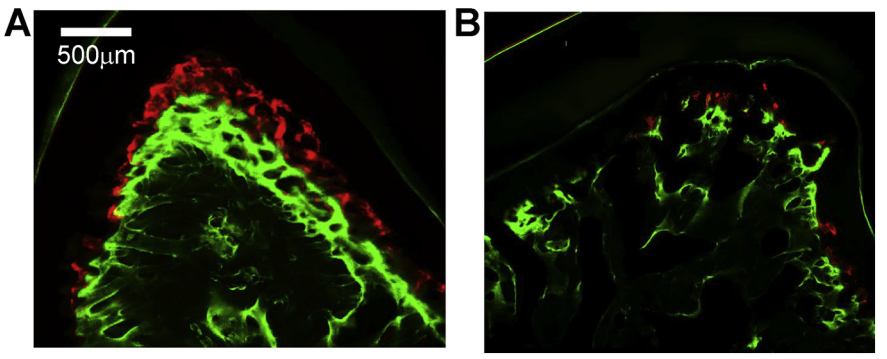

Fig. 8. Typical presentation of labeled fluorescent bands in the region underneath the root furcation. A: periodontal healthy sample (CG); B: periodontal disease sample (PGa).

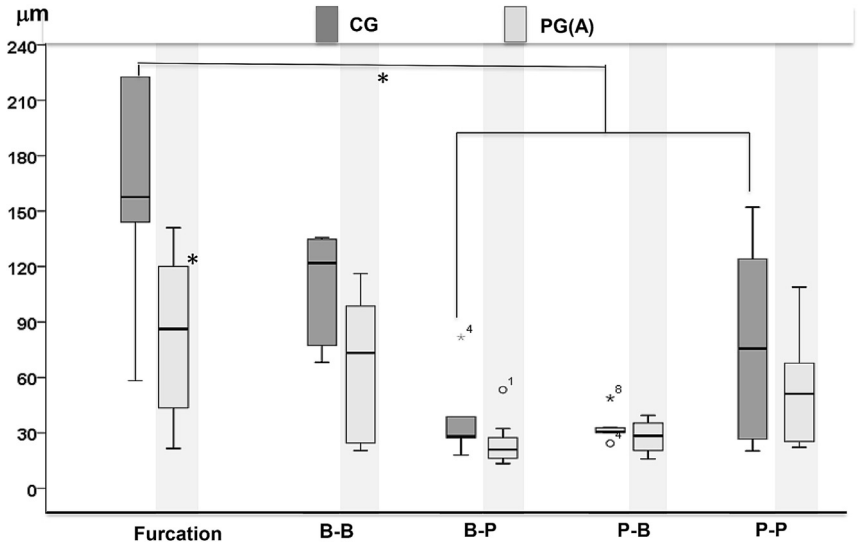

Fig. 9. Boxplot comparisons of mineral apposition rates (MARs) between induced periodontal disease (PGa) and control (CG) animals. Upper and lower limits of box represent 75th and 25th percentiles of each region, respectively. The upper and lower whiskers represent scores outside the middle 50%. Furcation: the region underneath the root furcation; B-B and B-P: buccal and palatal surfaces of buccal ridge respectively; P-B and P-P: buccal and palatal surfaces of palatal ridge respectively. Symbols outside box represent outlier (*o*) or extreme values (*). Horizontal line in each box represents median of the MAR. Asterisks indicate $p < 0.05$ when PGa was compared with CG.

greater on the outer than the inner surfaces of the alveolar ridge, i.e., buccal-buccal (B-B) and palatal-palatal (P-P) *vs* buccal-palatal (B-P) and palatal-buccal (P-B) surfaces. This difference implies that the mineralization of the outer surfaces of the alveolar ridges might be more active and also less perturbed by the induced periodontal disease than the inner surfaces. In each of the 4 animals receiving unilateral induction, comparison of MARs between the treated and control sides at the region underneath the root furcation further indicated reduced MAR by the induced periodontal disease (Fig. 10).

https://doi.org/10.1016/j.heliyon.2018.e00589

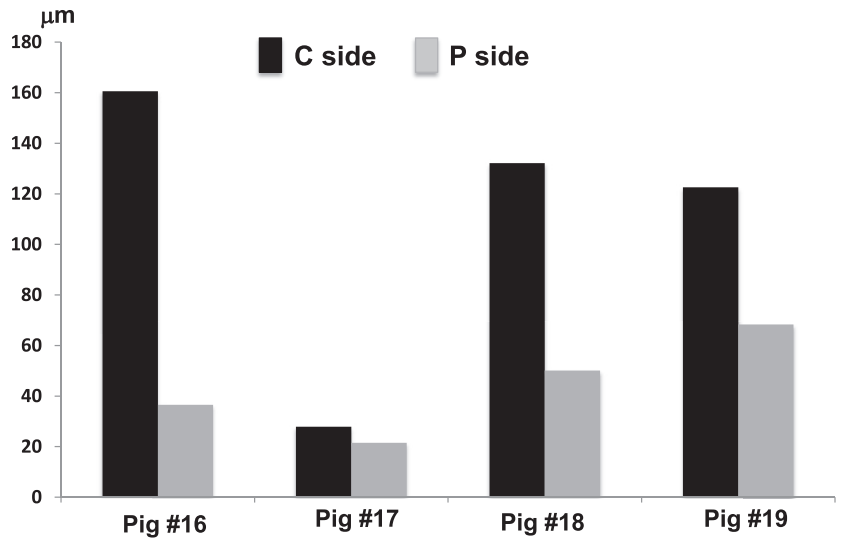

Fig. 10. Comparisons of mineral apposition rates (MARs) in 4 animals receiving the unilateral induction (split-mouth experiment). C and P sides represent the MAR values in control and induced sides of the target molar, respectively.

3.4. Association between alveolar bone mass and mineralization

Significant correlations were found between MARs of the alveolar ridge and volumetric measurements of the alveolar bone in the CG only. The MARs were positively associated with the volumes of total alveolar bone (TAB) and the palatal ridge (PAR, $p < 0.05$), and a similar tendency was also seen with the volume of the buccal ridge (BAR, Fig. 11A and B). However, this positive association was only found between the MARs and the volumes of total alveolar bone (TAB) in the PGa ($p < 0.05$, Fig. 11C).

4. Discussion

As a hallmark of periodontal disease, alveolar bone loss and its mechanism in relation to molecular pathways and mechanical traumas have been extensively examined in a number of studies (Henderson and Kaiser, 2018; Hienz et al., 2015). Distinctive from other bones, alveolar bone turns over very rapidly and is lost in the absence of a tooth. Therefore, the local environmental factors play a more important role in the homeostasis of alveolar bone (Nanci and Bosshardt, 2006). In periodontal disease, a local immunoinflammatory reaction to periodontal pathogens lead to alveolar bone loss. The occurrence of this bone loss is dependent upon two critical factors: 1) sufficient concentration of inflammatory mediators leading to the activation of the bone resorption pathway; 2) inflammatory mediators penetrating the gingival barrier (junctional epithelium) to reach within a critical distance to the alveolar bone (Cochran, 2008). Thus, the homeostasis of alveolar bone is perturbed with

https://doi.org/10.1016/j.heliyon.2018.e00589

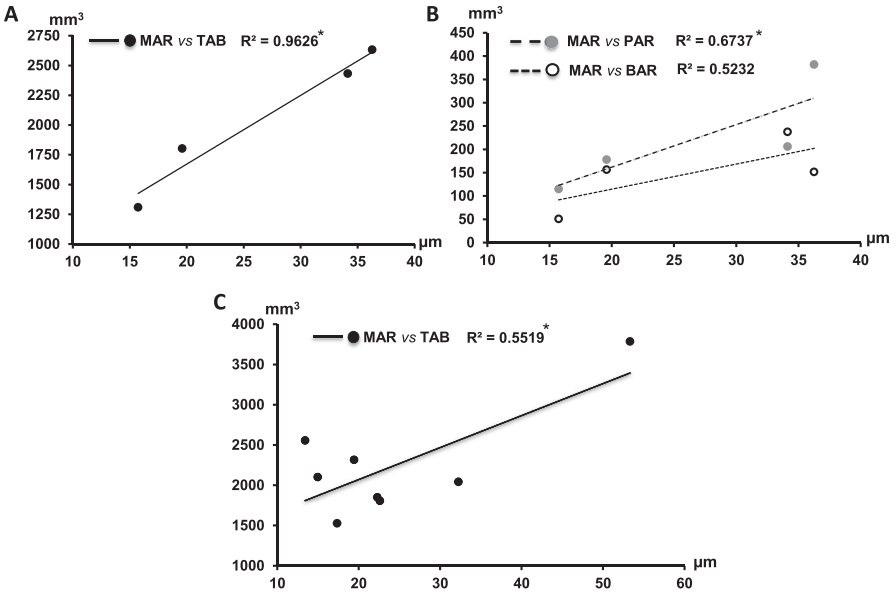

Fig. 11. Correlation between mineral apposition rates (MARs) of alveolar ridge and volumes of alveolar bone. A: MAR *vs* volume of total alveolar bone (TAB) in the control (CG); B: MAR *vs* volumes of palatal alveolar ridge (PAR) and buccal alveolar ridges (BAR) in the control (CG); C: MAR *vs* volume of total alveolar bone (TAB) in the experimental periodontal disease (PGa). Asterisks above the correlation coefficients (R^2) indicate $p < 0.05$, significantly correlated.

more bone resorption and less bone remodeling. Along with the damage of tooth supporting structures − periodontium, the loss and/or alteration of teeth further promote the breakdown of periodontium through occlusal trauma. The current pig model of experimental periodontal disease was designed to simulate this progress, even though the occlusal traumas and molecular pathways were not examined. However, the following two potential implications demonstrate the translational value of the present study; 1) due to the similarity of teeth, jaw, and oral function between pigs and humans, plus their comparable size, this established pig model of experimental periodontal disease may greatly benefit the studies on periodontal disease, in particular for those functional or biomechanical studies which require *in vivo* instrumentations and for evaluation of some newly developed interventions for treating or preventing periodontal disease; 2) the characteristics of alveolar bone loss and mineral apposition identified in this pig model may encourage the clinicians to pay closer attention to these regional differences during normal growth and the course of periodontal disease.

CBCT has proven to be an accurate tool to evaluate periodontal defects in a 3D format (Misch et al., 2006; Pinsky et al., 2006; Sun et al., 2011). The present CBCT 3D results clearly indicate that experimental periodontal disease caused significant reduction of alveolar bone, but the buccal side seemed to be less affected. In addition, the current study also found that the mass of the target molar roots was also

https://doi.org/10.1016/j.heliyon.2018.e00589

significantly reduced (Fig. 7). External root resorption in periodontal disease has been infrequently reported. The mechanism could be that bacteria penetrate patent dentinal tubules, and exit apical to the epithelial attachment. Consequently, the damaged area of the root surface is colonized by hard tissue resorbing cells, which penetrate into dentin through a small, denuded area, causing the resorption inside the root to spread. With time, the process may penetrate into the root canal (Fuss et al., 2003). However, based on micro-CT images and serial sections of histology, the resorption of the roots in the present study most likely occurred at the apical region (unpublished results).

During the homeostatic process of bones, mineral apposition is essential for the hardness and strength of newly formed bones, and is a series of physicochemical and biochemical processes in which crystals of calcium phosphate are produced by bone-forming cells and laid down in precise amounts within the bone matrix. This process facilitates the deposition of hydroxyapatite (HA) in specific areas of the extracellular matrix (ECM) (Millan, 2013). The bone labeling agents used in the present study, Calcein and Alizarin, have the capacity to chelate with the produced calcium in the process of mineral apposition, thus the mineral apposition rate (MAR) can be quantified. Given the fact that the characteristics of the mineralization process in the alveolar bone has not been well reported either in healthy or diseased conditions, the present study leads to the following four important findings (Figs. 8, 9, and 10): 1) mineralization amount is region specific during normal growth and remodeling of alveolar bone. The largest amount of mineral apposition occurs at the region underneath the root furcation, indicating that this region has more active bone growth and remodeling. The ongoing eruption of the permanent molar seems to have fewer influences on this feature because the permanent molar bud is distal to the last deciduous molar the present study targeted. However, this regional feature was not seen in periodontal disease; 2) there is a trend that more mineral apposition occurred in the outer (B-B and P-P) than inner (B-P and P-B) surfaces of alveolar ridges, indicating more new bone formation in the outer than the inner part of alveolar ridges regardless of periodontal healthy or diseased conditions; 3) even though there is significant bone loss in periodontal disease, the significant decrease of mineral apposition amount was only seen in the region underneath the root furcation. This feature indicates that either this region might undergo less new bone formation or the mineral apposition process itself was perturbed. Since the bone mass of this region was not measured in the present study, the potential mechanism cannot be explained; 4) a positive association between the mass of alveolar ridge and mineral apposition rate existed during the normal growth, but this association vanished in periodontal disease. To our best knowledge, no report has investigated such an association.

To maintain strength and mineral homeostasis, bone remodeling occurs throughout life and involves continuous removal of discrete packets of old bone, replacement

https://doi.org/10.1016/j.heliyon.2018.e00589

of these packets with newly synthesized proteinaceous matrix, and subsequent mineralization of the matrix to form new bone (Clarke, 2008). Therefore, larger bone mass may indicate more mineral apposition. The mass-mineral relationship of the mandible has been studied in healthy humans, but only bone mineral density (BMD) was calculated (Jonasson et al., 2007). Given the invasive nature of the bone labeling approach, measuring the mineral apposition rate *in vivo* is not possible in humans. The correlation analyses of the present study confirmed that a larger total alveolar bone mass was associated with a larger amount of mineral apposition in both periodontal healthy and diseased conditions. Furthermore, the positive correlation between the alveolar ridge mass and the amount of mineral apposition was only seen in periodontal healthy but not diseased conditions (Fig. 11). The possible explanation for this difference may be attributed to the fact that the alveolar ridge is the most affected area by periodontal disease, secondary to the region underneath the root furcation, where the mineralization could be perturbed or inhibited. In the present study, since the defined alveolar ridge (2.5 mm from the CEJ) only takes up about 1/5 of the defined total alveolar bone (CEJ to 2 mm below the root apex), it is reasonable to speculate that the process of mineral apposition in the portion of alveolar bone below the alveolar ridge might have not been perturbed by experimental periodontal disease (compare Fig. 7A, B to C).

The limitations of the present study include 1) relatively small sample sizes, especially for some of MAR measurements; 2) use of the last deciduous molar, rather than a permanent one. There are two reasons why the deciduous molar was chosen. The first is that the pig has to reach 7−8 months old to have the fully erupted first permanent molar. Since farm pigs were used in this study, it would be very difficult to handle the farm pigs during this age due to their size and weight (usually over 120 kg). The second is that the eruption location of the first permanent molar is distal to the existing last deciduous molar, rather than underneath the existing deciduous ones as for permanent premolars, canines, and incisors, thus the alveolar bone of the last deciduous molar is not supposed to be affected by the eruption process; 3) the present study investigated the MAR of alveolar bone which is part of the process of bone formation. However, no effort has been made to address the process of alveolar bone resorption. Therefore, the whole picture of bone remodeling or homeostasis in the induced periodontal disease has not been addressed by the present study.

In summary, the present study reached the following conclusions: 1) during normal alveolar bone growth and remodeling in young pigs, the region underneath the furcation of molar roots is the most active area of mineral apposition, and the outer surfaces of the alveolar ridge has more mineral apposition than the inner surfaces of the alveolar ridge; 2) experimental periodontal disease causes significant volumetric reduction of both alveolar bone and tooth roots, in which the palatal

https://doi.org/10.1016/j.heliyon.2018.e00589

alveolar ridge is affected more than the buccal alveolar ridge; 3) the alveolar region underneath the furcation of molar roots is not only the region showing the most active mineral apposition, but also a region where the mineral apposition is most affected by experimental periodontal disease; 4) in both periodontal healthy and diseased conditions, the mass of total alveolar bone is positively associated with the amount of its mineral apposition, but the association between the mass of alveolar ridge and amount of its mineral apposition is lacking in periodontal disease.

Declarations

Author contribution statement

Mandee Yang, Grace Eun Nam: Analyzed and interpreted the data; Contributed reagents, materials, analysis tools or data; Wrote the paper.

Atriya Salamati: Performed the experiments; Contributed reagents, materials, analysis tools or data.

Michael Baldwin, Mengzhao Deng: Analyzed and interpreted the data.

Zi-Jun Liu: Conceived and designed the experiments; Wrote the paper.

Funding statement

This work was supported by grant R21 DE023127 to ZJL and University of Washington Sunstar Preventative Dentistry Award to AS.

Competing interest statement

The authors declare no conflict of interest.

Additional information

No additional information is available for this paper.

Acknowledgements

The authors thank Dr. Jie Chen and Xianqin Bai for their helps with the experiments and histology, Dr. Johan Aps for his helps with CBCT imaging, and Dr. Sue Herring for constructive comments. Parts of this study were presented at the 94th General Session of International Association of Dental Research (IADR), Seoul, Korea, June, 2016, and Annual Meeting of American Society of Bone and Mineral Research (ASBMR), Atlanta, Sep, 2016.

https://doi.org/10.1016/j.heliyon.2018.e00589

References

Anderson, D.L., Thompson, G.W., Popovich, F., 1977. Tooth, chin, bone and body size correlations. Am. J. Phys. Anthropol. 46 (1), 7−11.

Clarke, B., 2008. Normal bone anatomy and physiology. Clin. J. Am. Soc. Nephrol. 3 (Suppl. 3), S131−139.

Cochran, D.L., 2008. Inflammation and bone loss in periodontal disease. J. Periodontol. 79 (8 Suppl.), 1569−1576.

Dahlberg, G., 1940. Statistical Method for Medical and Biological Students. Interscience Publications, New York.

Dempster, D.W., Compston, J.E., Drezner, M.K., Glorieux, F.H., Kanis, J.A., Malluche, H., Meunier, P.J., Ott, S.M., Recker, R.R., Parfitt, A.M., 2013. Standardized nomenclature, symbols, and units for bone histomorphometry: a 2012 update of the report of the ASBMR histomorphometry nomenclature committee. J. Bone Miner. Res. 28 (1), 2−17.

Di Benedetto, A., Gigante, I., Colucci, S., Grano, M., 2013. Periodontal disease: linking the primary inflammation to bone loss. Clin. Dev. Immunol. 2013, 503754.

Farquharson, D., Butcher, J.P., Culshaw, S., 2012. Periodontitis, porphyromonas, and the pathogenesis of rheumatoid arthritis. Mucosal Immunol. 5 (2), 112−120.

Fuss, Z., Tsesis, I., Lin, S., 2003. Root resorption−diagnosis, classification and treatment choices based on stimulation factors. Dent. Traumatol. 19 (4), 175−182.

Gingerich, P.D., 1977. Correlation of tooth size and body size in living hominoid primates, with a note on relative brain size in aegyptopithecus and proconsul. Am. J. Phys. Anthropol. 47 (3), 395−398.

Henderson, B., Kaiser, F., 2018. Bacterial modulators of bone remodeling in the periodontal pocket. Periodontol. 2000 76 (1), 97−108.

Herring, S.W., Li, Y.M., Liu, Z.J., Popowics, T.E., Rafferty, K.L., Wang, S.L., 2011. The minipig in biomedical research. In: McAnulty, P.A., Dayan, Anthony D., Ganderup, N.-C., Hastings, K.L. (Eds.), Oral Biology and Dental Models. CRC Press, Taylor & Francis Group, London, New York.

Hienz, S.A., Paliwal, S., Ivanovski, S., 2015. Mechanisms of bone resorption in periodontitis. J. Immunol. Res. 2015, 615486.

Jonasson, G., Jonasson, L., Kiliaridis, S., 2007. Skeletal bone mineral density in relation to thickness, bone mass, and structure of the mandibular alveolar process in dentate men and women. Eur. J. Oral Sci. 115 (2), 117−123.

https://doi.org/10.1016/j.heliyon.2018.e00589

Liu, Z.J., King, G.J., Herring, S.W., 2006. Condylar mineralization following mandibular distraction in rats. J. Dent. Res. 85 (7), 653–657.

Meng, H., Xie, H., Chen, Z., 1996. Evaluation of ligature-induced periodontitis in minipig. Zhonghua Kou Qiang Yi Xue Za Zhi 31 (6), 333–336.

Millan, J.L., 2013. The role of phosphatases in the initiation of skeletal mineralization. Calcif. Tissue Int. 93 (4), 299–306.

Misch, K.A., Yi, E.S., Sarment, D.P., 2006. Accuracy of cone beam computed tomography for periodontal defect measurements. J. Periodontol. 77 (7), 1261–1266.

Nanci, A., Bosshardt, D.D., 2006. Structure of periodontal tissues in health and disease. Periodontol. 2000 40, 11–28.

Oz, H.S., Puleo, D.A., 2011. Animal models for periodontal disease. J. Biomed. Biotechnol. 2011, 754857.

Pinsky, H.M., Dyda, S., Pinsky, R.W., Misch, K.A., Sarment, D.P., 2006. Accuracy of three-dimensional measurements using cone-beam ct. Dentomaxillofac. Radiol. 35 (6), 410–416.

Rodan, G.A., 1998. Bone homeostasis. Proc. Natl. Acad. Sci. U. S. A. 95 (23), 13361–13362.

Rodan, G.A., Martin, T.J., 2000. Therapeutic approaches to bone diseases. Science 289 (5484), 1508–1514.

Sun, Z., Smith, T., Kortam, S., Kim, D.G., Tee, B.C., Fields, H., 2011. Effect of bone thickness on alveolar bone-height measurements from cone-beam computed tomography images. Am. J. Orthod. Dentofac. Orthop. 139 (2), e117–127.

Yushkevich, P.A., Piven, J., Hazlett, H.C., Smith, R.G., Ho, S., Gee, J.C., Gerig, G., 2006. User-guided 3d active contour segmentation of anatomical structures: significantly improved efficiency and reliability. Neuroimage 31 (3), 1116–1128.

https://doi.org/10.1016/j.heliyon.2018.e00589